A Photochemical and Electrochemical Triggered Bis(hydrazone) Switch

Article *in* Chemistry - A European Journal · April 2018

DOI: 10.1002/chem.201703065

CITATIONS
4

READS
213

6 authors, including:

Mónica Soto-Monsalve

18 PUBLICATIONS **14** CITATIONS

SEE PROFILE

Christian Camilo Carmona-Vargas

University of Strasbourg

11 PUBLICATIONS **69** CITATIONS

SEE PROFILE

Richard Fernando D'vries

Universidad Santiago de Cali

56 PUBLICATIONS **374** CITATIONS

SEE PROFILE

Gustavo Gutiérrez-Gómez

University ICESI

8 PUBLICATIONS **13** CITATIONS

SEE PROFILE

CHEMISTRY
A European Journal

A Journal of
ChemPubSoc Europe

Accepted Article

Title: A Photochemical and Electrochemical Triggered Bis(hydrazone) Switch

Authors: Mónica A. Gordillo, Mónica Soto-Monsalve, Christian C. Carmona-Vargas, Gustavo Gutierrez, Richard F. D'vries, Jean-Marie Lehn, and Manuel N. Chaur

To be cited as: *Chem. Eur. J.* 10.1002/chem.201703065

Link to VoR: http://dx.doi.org/10.1002/chem.201703065

Supported by
ACES

WILEY-VCH

10.1002/chem.201703065

WILEY-VCH

FULL PAPER

A Photochemical and Electrochemical Triggered Bis(hydrazone) Switch

Mónica A. Gordillo,[a] Mónica Soto-Monsalve,[b] Christian C. Carmona-Vargas,[a] Gustavo Gutiérrez,[c] Richard F. D´vries,[d] Jean-Marie Lehn,[e] and Manuel N. Chaur*[a]

Abstract: Herein, we report the synthesis of a double hydrazone capable of undergoing photochemical *E*/*Z* isomerization through the imine double bonds. The bis(hydrazone) **1-*E,E*** can be considered as a "two-arm" system in which the controlled movement of each arm is obtained by photo-modulation, making possible the appearance of two isolable metastable isomeric states **1-*E,Z*** and **1-*Z,Z***. Such states are characterized by very specific structural, optical and electrochemical properties. The latter, allows the reversible return from either **1-*E,Z*** or **1-*Z,Z*** to the **1-*E,E*** state. Our results are of great importance in the further development of molecular machines and photochemically controlled reactions by introducing for the first time double hydrazones as tunable photochemical switches.

Introduction

Over the past two decades, the design and construction of molecular machines[1–3] that can act like molecular switches,[4,5] brakes,[6–8] and motors[9] have been developed, inspired by their natural, macroscopic and biological analogues,[10] attracting a great interest for the advancement in the nanotechnology field.[11] In fact, the art of building small molecular machinery which motions can be directed in a controlled manner from the outside was awarded with the Nobel Prize to Sir Fraser Stoddart, Jean-Pierre Sauvage and Ben Feringa in 2016.

The appropriate assembly of the molecular components, that interacts with light whether in a reversible or irreversible fashion, with the ability of performing a task is usually called a photochemical molecular device.[12] Therefore, supramolecular systems designed to undergo a mechanical motion by configurational, and conformational changes upon light irradiation can be defined as photochemical molecular machines.[13]

[a] M. A. Gordillo, C.C. Carmona-Vargas, Prof. Dr. M. N. Chaur
Departamento de Química, Facultad de Ciencias Naturales y Exactas, Universidad del Valle, A.A 25360, Cali, Colombia
E-mail: manuel.chaur@correounivalle.edu.co
[b] M. Soto-Monsalve
Instituto de Química de São Carlos, Universidade de São Paulo, 13566-590, São Carlos, Brazil
[c] G. Gutierrez
Departamento de Ciencias Farmacéuticas, Universidad Icesi, Cali, Colombia
[d] Prof. Dr. R.F. D´Vries
Facultad de Ciencias Básicas, Universidad Santiago de Cali, Cali, Colombia.
[e] Prof. Dr. J-M. Lehn
Laboratoire de Chimie Supramoléculaire, Institut de Science et d'Ingéniere Supramoléculaires, Université de Strasbourg, 8 Allée Gaspard Monge, 67000, Strasbourg, France

Supporting information for this article is given via a link at the end of the document.

Examples of these light-driven machines can be found in compounds containing substituted double bonds like N=N present in azo compounds,[14] and C=N present in imines, oximes[15] and hydrazones.[16] Among these compounds, molecular strands possessing alternating hydrazone and heterocyclic units such as pyrimidine,[17] pyridine,[18] and triazine[19] have particular attention by their applications in the development of nanometric devices.[20] The hydrazone straightforward methodology of synthesis, by the condensation of hydrazine and aldehyde derivatives of the desired heterocyclic core,[21,22] makes them very accessible.

On the other hand, hydrazones derived from 2-pyridinecarbaldehyde (as well as related acylhydrazones) are triple dynamic entities capable of undergoing both, configurational dynamics, by *E*-*Z* photoisomerization reactions,[23,24] as well as, conformational dynamics by pH changes[25,26] or metal ion binding [6,27–29] Therefore, these kind of hydrazones show potential applications for the development of supramolecular systems for molecular motion (switches,[30,31] tweezers,[32] walkers,[33] etc.) and information storage devices (catenanes,[34] racks,[35] metallogrids,[36] and combinatorial dynamic libraries[27,37]).

The dynamics of hydrazone compounds have been widely studied in the last decade by Lehn's group.[23,27,29] It has been reported that light-driven isomerization of these imine systems may convert the thermodynamically most stable *anti* (*E*) isomer to the less stable (metastable) *syn* (*Z*) isomer by the out of plane rotation around the C-N bond *via* a perpendicular transition state, or by the in-plane imine nitrogen inversion *via* a linear transition state.[15,38,39] Moreover, Aprahamian and co-workers showed that the mechanism of acid-catalyzed isomerization of hydrazones with intramolecular hydrogen bonds goes through an azo-hydrazone tautomerism and rotation of a single C-N bond.[40]

However, the photochemical study of hydrazone systems have been limited to acylhydrazones,[24] aroylhydrazones,[41] and tricarbonyl-2-arylhydrazones[40], with a single C=N unit, leaving aside hydrazone systems with more than one C=N fragment. Therefore, extending the photochemical studies to molecular strands with a higher number of imine bonds, may lead to the development of novel functional systems and materials through light-induced configurational switching processes.

Recently, we have reported the synthesis of the bis(hydrazone) **1-*E,E*** which is highly soluble in organic solvents due to the long alkyl chain attached to the thiopyrimidine ring. This bis(hydrazone) undergoes conformational changes from *transoid* to *cisoid* through coordination to transition metal ions (Co^{2+}, Ni^{2+}, Zn^{2+}).[42] Hence, we envisioned that **1-*E,E*** could also undergo configurational motion by the isomerization of the two C=N bonds, even more, controlling such isomerization would allow the manipulation of movement in the molecule to desire.

10.1002/chem.201703065

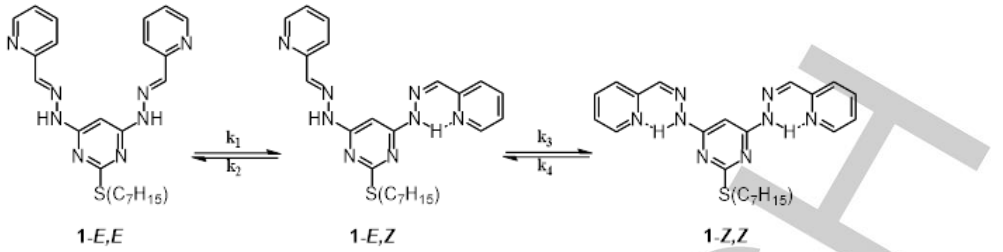

Scheme 1. Formation of the three different configurational isomers of bis(hydrazone) **1-*E,E*** by UV light irradiation following a consecutive two-step reaction with both steps being reversible kinetics.

To the best of our knowledge, there is no report on the physicochemical properties of configurational isomers of bis(hydrazones), thus, the electronic properties, considered for information storage and electronic applications have been unexplored so far. Herein, we describe the isolation, structural characterization, and study of the photophysical and electrochemical properties of the configurational isomers (Scheme 1) of (*E,E*)–pyridine–2–carboxaldehyde–[2–heptylthiopyrimidine–4,6–diyl]bishydrazone (**1-*E,E***). In addition, the kinetics of the photoisomerization process and the conversion of each isomer were monitored by ^{1}H Nuclear Magnetic Resonance (NMR), and confirmed by single crystal X-ray diffraction. DFT calculations were also performed to estimate the hydrogen bond energy in the isomers **1-*E,Z*** and **1-*Z,Z***.

Abstract in Spanish: *En este trabajo presentamos la síntesis de una doble hidrazona capaz de experimentar isomerización fotoquímica E/Z a través de los dobles enlaces imina. La bis(hidrazona)* ***1-E,E*** *puede ser considerada como un sistema de "dos brazos" en el cual el movimiento controlado de cada brazo es obtenido por foto-modulación, siendo posible la aparición de dos estados isoméricos metaestables* ***1-E,Z*** *y* ***1-Z,Z****. Los 3 isómeros están caracterizados por sus propiedades estructurales, ópticas y electroquímicas. El estudio de estas últimas, muestra el retorno de manera reversible de los estados* ***1-E,Z*** *o* ***1-Z,Z*** *al estado* ***1-E,E****. Nuestros resultados son de gran importancia para el desarrollo de máquinas moleculares y reacciones controladas fotoquímicamente, presentando por primera vez hidrazonas dobles como interruptores fotoquímicos manipulables*.

Results and Discussion

Photoisomerization of (*E,E*)–Pyridine–2–carboxaldehyde–[2–heptylthiopyrimidine–4,6–diyl]bishydrazone (1-*E,E*): A 26.5 mmol.L^{-1} solution of the bis(hydrazone) **1-*E,E*** in an NMR Quartz tube was placed at 20 cm away from a 250 W mercury-vapour lamp (radiant power 9.23x10^{-6} E·s^{-1}·dm^{-3}). Each isomer obtained from the UV irradiation of the bishydrazone **1-*E,E*** in commercial acetone was isolated by column chromatography using a gradient of elution from $CHCl_3$ to $CHCl_3$/MeOH 3%.

Figure 1 shows the expanded region of the stacked ^{1}H NMR spectra of **1-*E,E***, through the irradiation time, as well as the signals of the forming configurational isomers. These data were used to quantify the percentage of **1-*E,Z*** and **1-*Z,Z***, taking as reference the characteristic signal of the hydrogen at the C5 of the pyrimidine ring of **1-*E,E***, with a chemical shift at 6.93 ppm in deuterated acetone. This signal was taken as reference since the emerging signals corresponding to the **1-*E,Z*** and **1-*E,Z*** isomers can easily be distinguished and do not overlap with that of **1-*E,E***.

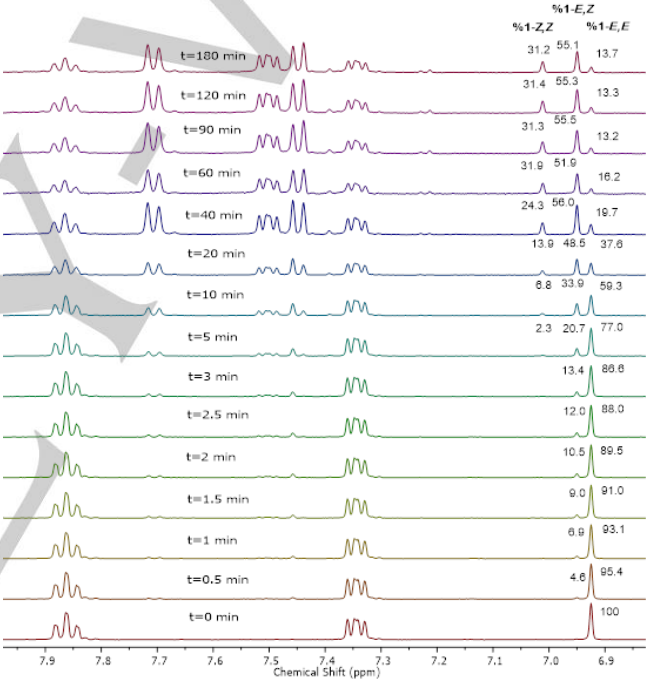

Figure 1. A portion of the stacked ^{1}H NMR spectra of the bis(hydrazone) **1-*E,E*** irradiated with UV light at different times . The concentration of the solution was 26.75 mmol.L^{-1} in acetone-d_6, and the radiant power calculated was 9.23x10^{-6} E·s^{-1}·dm^{-3}.

As going from bottom to top in Figure 1, it is observed the emergence of new signals corresponding to the just formed configurational isomers 1-***E,Z*** and 1-***Z,Z***. The value of the integral of the aforementioned signals can be related to the concentration of the starting compound, being possible to obtain the evolutions of concentration in time for the different isomers (Figure 2). Then, by fitting the experimental data with several kinetic models using the Dynafit[43] software, it was found that the kinetics of photoisomerization of this system indicates a consecutive two-step reaction with both steps being reversible (Scheme 1).

10.1002/chem.201703065

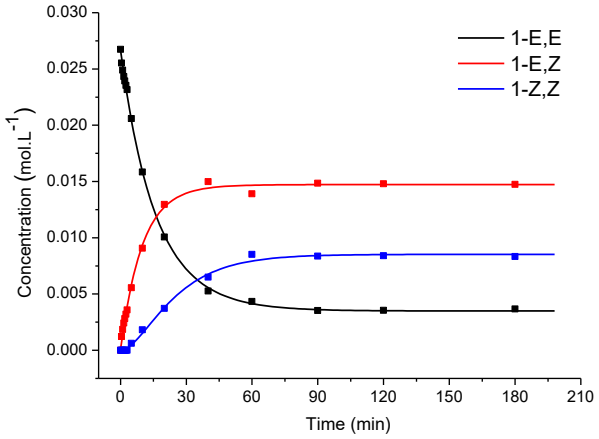

Figure 2. Experimental (dots) and fitted (line) time profile of each isomer.

The experimental time profile (dots) and the best-fit time profile (line) for each isomer are shown in Figure 2. The resulting rate constants for the photoisomerization processes are k_1 = 0.0561 ± 0.0009 min^{-1}, k_2 = 0.0133 ± 0.0006 min^{-1}, k_3 = 0.034 ± 0.003 min^{-1} and k_4 = 0.059 ± 0.005 min^{-1}. These results show that both equilibria are shifted towards the **1-*E,Z*** isomer formation, which is in accordance with the isomers distribution when the isolated **1-*Z,Z*** is irradiated under the same conditions, where again, **1-*E,Z*** is the main product obtained with the highest yield of conversion, also proving the reversibility of the reaction. Additionally, these isomers (**1-*E,Z*** and **1-*Z,Z***) are resistant to the reverse thermal isomerization processes in the absence of UV irradiation, since there was no change in the percentage of the isomers in a solution stored during 3 days at 30 °C, neither when the solution was heated at 45 °C during 8 hours. Addition of trifluoroacetic acid (TFA) and heat (45°C) during 8 hours leads to the back conversion to the **1-*E,E*** isomer. These facts demonstrate the high stability that the intramolecular hydrogen bond provides to the configurational isomers. Indeed, our DFT calculations show a high value of the hydrogen bond energy (*vide infra*).

NMR spectroscopic features of the configurational isomers: When comparing the ^{1}H NMR spectra of the isomers **1-*E,E*** and **1-*E,Z***, it can be observed an increase in the number of signals in the aromatic region due to the loss of symmetry of the molecule. The proton 5 that belongs to the pyrimidine ring is shifted to lower field than its analogue in **1-*E,E***, since in this new configuration it is deshielded by the proximity of this proton to the C=N bond of the isomerized unit.[35] The same behaviour is observed for **1-*Z,Z*** as can be seen in the figure 3, where this effect is more pronounced resulting in a lower field shifting of the proton.

On the other hand, due to the intramolecular hydrogen bond formed in the **1-*E,Z*** isomer, the –N-H proton involved in this bond is quite deshielded and therefore, it is shifted to low field. The remaining signals were assigned from the information given by the two-dimensional experiments COSY and HSQC (see supplementary information).

The symmetry of the **1-*Z,Z*** isomer is reflected in the smaller number of signals of its spectrum (Figure 3), besides the aforementioned low-field shift of the C5 proton. Each signal in the region ranging from 7.45 to 8.81 ppm integrates for two protons, evidencing the gain in symmetry when this configuration is adopted. In addition, the signal at 14.0 ppm, which corresponds to the protons involved in the hydrogen bond integrate for two protons, confirming the two hydrogen bonds formed in this configuration.

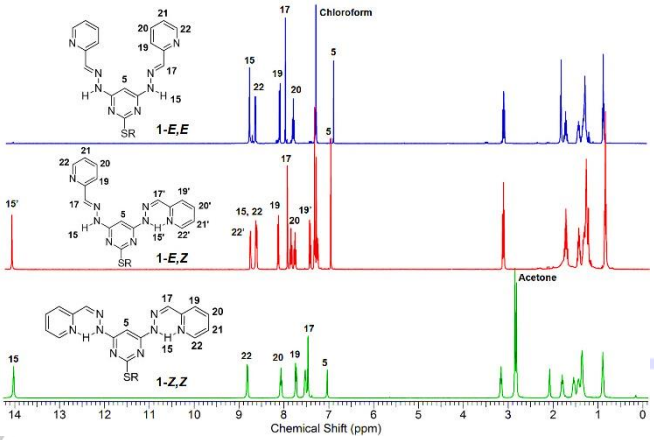

Figure 3. ^{1}H-NMR spectrum of isomers **1-*E,E***, **1-*E,Z***, in $CDCl_3$ and **1-*Z,Z*** in acetone-d_6.

X-Ray Crystallographic studies: In order to obtain single crystals, several slow evaporation experiments in acetone and methanol were performed. The obtained single crystals were fully characterized by X-ray crystallography (Figure 4, see SI Table S1) confirming the configuration adopted by each isomer.

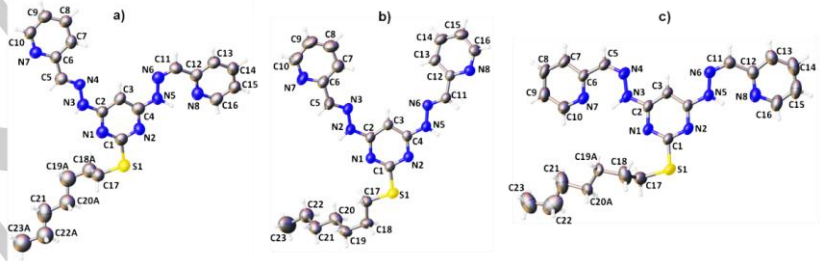

Figure 4. ORTEP representation of the asymmetric unit of each configurational isomer, a) **1-*E,Z***, b) **1-*E,E*** and c) **1-*Z,Z***, of the -Pyridine–2–carboxaldehyde–[2–heptylthiopyrimidine–4,6–diyl]bishydrazone. Thermal ellipsoids are drawn at 50% probability level.

10.1002/chem.201703065

Isomer **1-*E,E*** crystallized in the monoclinic space group C2/c, **1-*E,Z*** crystallized in the orthorhombic space group *Pnab*, while **1-*Z,Z*** crystallized in the triclinic space group *P-1*. A symmetry loss in the crystal packing is observed due to the inherent conformational differences in the molecules, which generate in each particular case, characteristic intra and intermolecular interactions. Additionally, a typical configurational disorder was observed in the carbon atoms of the alkyl chains as it is shown in the structural superposition (Figure 5).

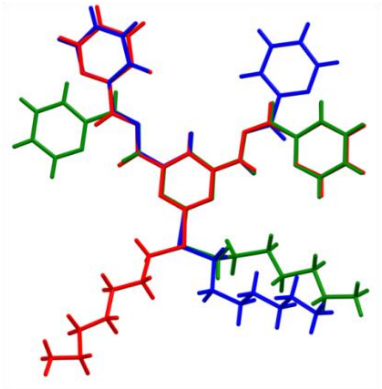

Figure 5. Structural superposition of the isomers **1-*E,Z*** (red), **1-*E,E*** (blue) and **1-*Z,Z*** (green).

It is possible to observe four differences in the three isomers such as (i) the increase in the torsion angles, in relation to the hydrazone bridge, in the order **1-*Z,Z*** < **1-*E,E*** < **1-*E,Z*** (see Table 1); (ii) the deviation in the dihedral angles of the pyridine rings; (iii) the high planarity deformation in the central pyrimidine ring in the order **1-*E,Z*** < **1-*Z,Z*** < **1-*E,E*** (see table 1), and (iv) the orientation of the aliphatic chain in different directions.

Table 1. Torsion angles, dihedral angles and ring puckering analysis for 1-***E,E***, 1-***E,Z*** and 1-***Z,Z***.

Head 1[a]	**1-*E,E***	**1-*E,Z***	**1-*Z,Z***
N7 – C6 – C5 – N4	172.82°	175.16°	-0.36°
N8 – C12 – C11 – N6	170.97°	12.23°	-1.01°
Ring 1-Ring 2	3.68°	12.76°	17.16°
Ring 1-Ring 3	19.77°	9.97°	11.95°
Ring 1 distortion	3.68°	0.65°	1.60°

[a] Ring 1= C1-N1-C2-C3-C4-N2; Ring 2= C6-C7-C8-C9-C10-N7; Ring 3= C12-C13-C14-C15-C16-N8

The supramolecular analysis for the three isomers reveals that these supramolecular networks are formed mainly by N-H···N hydrogen bonds and π-π stacking interactions between the aromatic rings (for more supramolecular details see the figures S14 – S16 in the supporting information).

Another way to observe the supramolecular interactions distribution of the three isomers is through Hirshfeld surfaces and the 2D fingerprints plots (Figure 6).[44–46] The Hirshfeld surface shows the susceptible areas to participate in interactions and the 2D fingerprint plots provide quantitative information about the contributions to the intermolecular interactions forming the crystal packing. As it is possible to observe in the Figure 9, the three isomers present differences in the form and distribution of the 2D fingerprint plots. This clearly indicates that each crystal packing is governed by a different distribution of supramolecular interactions. In all the cases, the van der Waals H···H interaction is the most abundant followed by the N···H, C···H and C···C interactions. The observed quantitative values are in agreement with the structural description, where N···H and C···H interactions give rise to the supramolecular packing (Figure 6c).

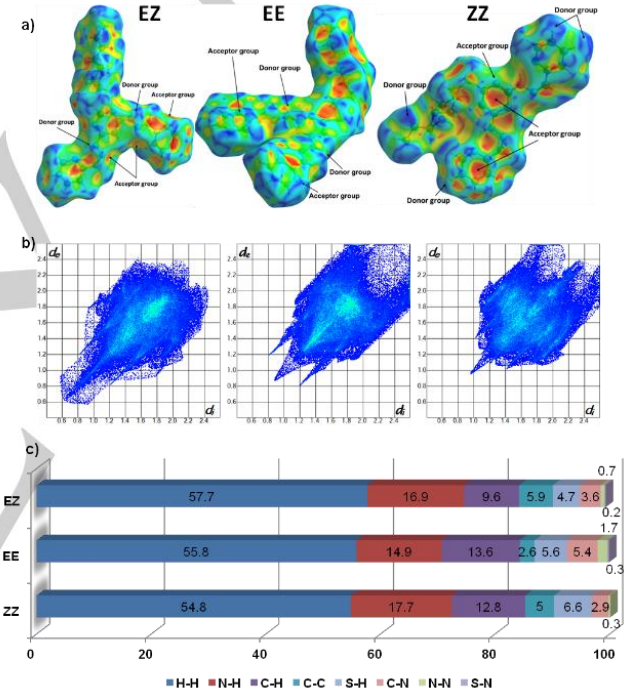

Figure 6. a) Hirshfeld surfaces, b) 2D- fingerprint plots and c) supramolecular interactions distribution for the isomers **1-*E,Z***, **1-*E,E*** and **1-*Z,Z***.

Hydrogen bond energy estimation via rotational barrier calculations: Even though the Møller–Plesset (MP) perturbation theory methods are the most used in hydrogen bond study, some authors have successfully used Density Functional Theory (DFT) approximation through Restricted Becke, Lee, Yang and Parr hybrid functional (B3LYP) methods for medium to large systems[47] in order to avoid costs of MP methods. Due to the aforementioned reasons, the optimization of the structure of each isomer was carried out using DFT/B3LYP: 6-311+G (d, p) (Table 2).

10.1002/chem.201703065

Table 2. Linear regression parameters for comparison of optimized and crystallographic molecular structures

	Bond length[a]				Bond angle			
Isomer	**%Error[b]**	**Slope**	**Intercept**	**R^2**	**%Error[b]**	**Slope**	**Intercept**	**R^2**
1-*E,E*	1.83	1.0592	-0.0737	0.98884	0.85	0.9593	4.9385	0.95279
1-*E,Z*	2.93	1.0663	-0.0873	0.98633	1.09	0.9013	12.185	0.92887
1-*Z,Z*	1.41	1,007	-0,0008	0.98540	0.99	0.9294	8.1937	0.9525

[a] Regressions exclude N–H bonds and heptyl substituent bond length parameters

[b] Average percentage error: whole data were included in average calculation

In order to carry out a systematic comparison between optimized and crystallographic structures, linear regression analyses were performed.[48] In this type of analysis, the slope represents a ratio among the set of variations of calculated-experimental data. The intercept corresponds to the value of the dependent variable (calculated) when the independent variable (experimental) is equals to zero: meaning an over or underestimation value. Thus, perfect correlation is given when the slope and intercept values are 1 and 0, respectively. The optimized structures at the DFT/B3LYP: 6-311+G (d, p) level of theory show good correlation with experimental data from X-ray diffraction (see Table 2 and Figure 7).

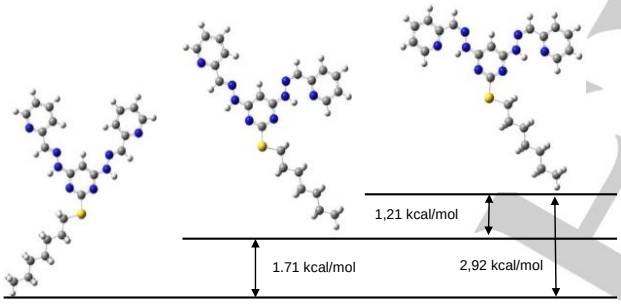

Figure 7. Optimized geometries and energy difference between **1-*E,E***, **1-*E,Z*** and **1-*Z,Z*** isomers.

Furthermore, root-mean-square deviation (RMSD) of atomic position values were computed for superposition of **1-*E,E***, **1-*E,Z***, and **1-*Z,Z***, for both experimental and calculated structures.[49] This parameter assesses how much two structures are homologous since RMSD is, by definition, the square root of the mean quadratic difference between the positions of each superposed atom. As shown in figure 8a, superposing the structures results in high RMSD ranging from 1.5 to 2.1 due to the observed deviations, which are attributable to the fluctuating alkyl chain orientation. This is supported by the structural superposition without the heptyl moiety (see Figure 8b) where RMSD values now range from 0.2 to 0.4 indicating good theoretical-experimental agreement. The discrepancies observed in the entire molecular structure are not an inconvenient since the molecular fragment involved in the rotational barrier calculations show good alignment and those calculations were carried out independently.

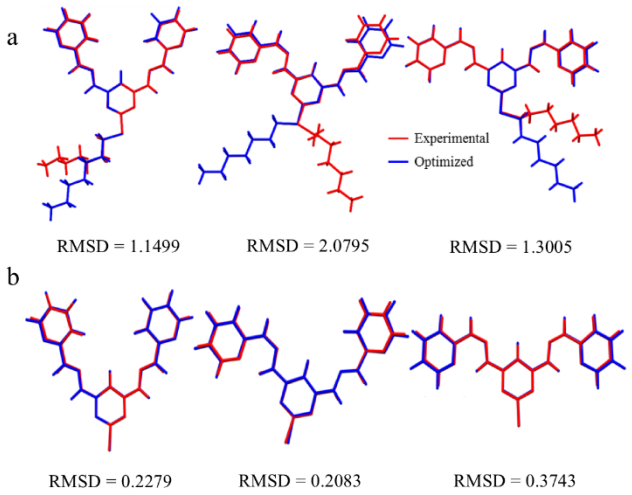

Figure 8. Superposition of the structures of the isomers. From left to right 1-***E,E***; 1-***E,Z***; and 1,***Z-Z***. **a**. Entire structures **b**. Structures without the heptyl moiety

Some studies on the acid-base properties,[50] infrared frequency shifts,[51] NMR coupling constants,[52] hydrogen bond length and angles, have been made in order to establish the relationship among the spectroscopic or structural features of compounds that exhibit hydrogen bonds. However, an interest in the use of theoretical methods for hydrogen bonding energy estimation has been developed in order to address the problem of determining the bond energy value directly through theoretical methods. *Ortho-Para,*[53] *isodesmic/homodesmic reactions*[54] and *conformational analysis approach* are some of these methods, however, each method presents some intrinsic limitations or inaccuracies. The *Ortho-Para approach* introduces a H–H steric hindrance in the planar conformation when pyridine nitrogen atom is transposed from 2- to 3- or 4-position.

On the other hand, dihedral angles different from zero represent local minima conformations in preliminary calculations. *Conformational analysis*[55] also known as *cis-trans approach* yielded a weak hydrogen bond of about 1.71 kcal/mol, and this energy value is not consistent with the high stability of **1-*E,Z*** and **1-*Z,Z*** isomers in solution. The molecular tailoring approach has been successfully and accurately applied to address the problem

10.1002/chem.201703065

of hydrogen bond strength calculations, since through hypothetical fragmentation of the system it is possible to estimate the energy associated with the H-bond by subtracting the energy of other interactions.[56] Nevertheless, we probed several partitioning models without obtaining reasonable results.

With the aim of applying an estimative approach to *measure* the hydrogen bond strength, the rotational energy profile of the dihedral angle between the hydrazone moiety and the pyridine ring was calculated at DFT/B3LYP: 6-311+G (d, p) level of theory since the relationship between both parameters was previously described (Figure 9).[57]

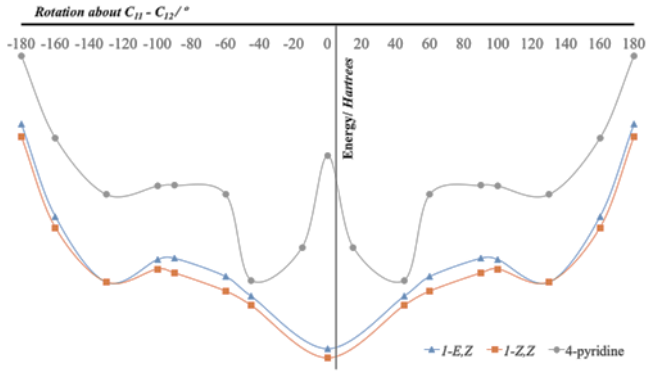

Figure 9. Rotational energy profile for pyridine ring rotation. Energy in each point is represented as relative energy respect to **1-*E,Z*** and **1-*Z,Z*** global minima energy, respectively.

As observed in figure 9, the dihedral angle rotational profile exhibits inflexion points at ~ 0, 100, 130, -100 and -130°. Inflexion at 0° corresponds to the global minima for both isomers where conformation allows the maximum possible N–H···N interaction. Although the IUPAC defines the rotational barrier as the energy barrier between two adjacent minima points, a rotation about C_{11}-C_{12} from -130º or 130° to 0° must overcome a local maximum at 90º, increasing the energy barrier and consequently, having a rotational barrier that corresponds to N–H···N interaction equals to 11.29 and 11.03 kcal/mol for **1-*E,Z*** and **1-*Z,Z***, respectively.

Likewise, the rotational energy profile was computed for an hypothetical 4-pyridine *E,Z* derivative (see Figure 9). The molecular model for the aforementioned compound is shown with the aim of clarifying the evaluated rotation, geometries showing different dihedral angles are indicated (see figure 10).

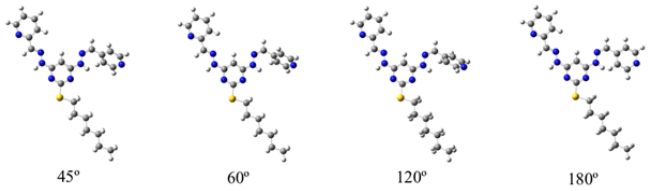

Figure 10. 4-pyridine *E,Z* derivative rotation way

Taking into account the effect of steric hindrance estimated for the hypothetical compound, over the rotational energy profile, the rotational barrier that corresponds to N–H···N interaction is equals to equals to 4.43 and 4.69 kcal/mol for **1-*E,Z*** and **1-*Z,Z***, respectively. These results remark the importance of the hydrogen bond formed by the interaction of the N-H group and the 2-substituted pyridine ring in compounds of this work.

So far, it has been remarked along the manuscript that the hydrogen bond stabilizes the *Z* configurations, and as result, the **1-*E,Z*** and the **1-*Z,Z*** isomers are described as metastable states capable of being interconverted only by UV radiation or high temperatures (>50 °C). However, electrochemical studies of these isomers open the possibility towards another way to interconvert these states (*vide infra*).

Absorption spectra: The *E*-to-*Z* configurational change of **1-*E,E*** that leads to the formation of **1-*E,Z*** and **1-*Z,Z*** can also be studied by UV spectroscopy. The UV-Vis spectra of the three isomers in chloroform (Figure 11) shows three bands between 280-366 nm, which are attributed mainly to π-π* transitions. Bands within the 280-285 nm range are characteristics of the C=N group of hydrazones and the other two absorption bands between 310-366 nm correspond to π-π* transitions of the pyridine and pyrimidine rings.[58] The most notable change in the spectrum of each isomer is the bathochromic shift of 9.0 nm and 22 nm for **1-*E,Z*** and **1-*Z,Z*** respectively, for the bands between 344-366 nm. A hyperchromic shift is observed in the band at 366 nm of the **1-*Z,Z***, and another bathochromic shift is seen in the region of 310-322 nm of 4.0 and 12 nm for **1-*E,Z*** and **1-*Z,Z*** respectively.

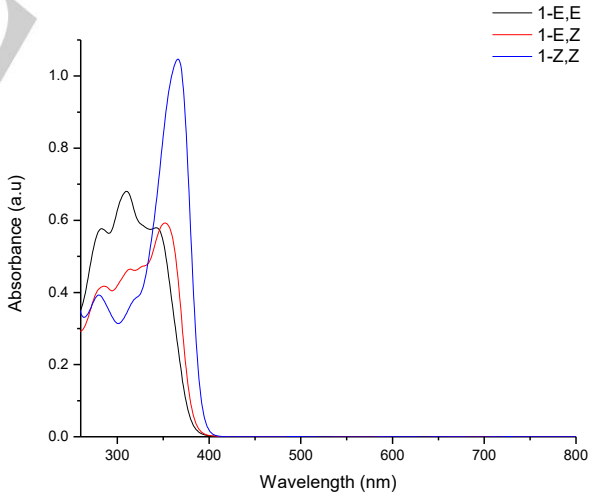

Figure 11. UV-Vis spectra of the three isomers in chloroform

The shifts are probably caused by the slightly extended conjugation between the pyridine ring, the C=N group and the pyrimidine ring. A pseudo six membered ring is formed by an intramolecular hydrogen bond, leading to a larger bathochromic shift for the **1-*Z,Z*** isomer than for the **1-*E,Z***, since the former has two intramolecular hydrogen bonds, corresponding to two pseudo

six membered rings and further extending the π-delocalization. The conjugation of the system is limited because the pseudo ring is not completely planar, for that reason the bathochromic shifts are not as large as for other similar systems found in the literature.[40,59,60] A similar behaviour for the three isomers is observed in dichloromethane and acetone, but due to the λ cut off of acetone only one band can be observed. Molar absorptivities and energy band gaps calculated using the spectral onsets are presented in table 3 for three different solvents.

Table 3. Results from the photophysical studies of the three isomers in various solvents

Solvent	Isomer	λ_{max} (nm)	ε (cm^{-1} M^{-1})	ΔE_{elec} (eV)
Chloroform	1-*E,E*	344	32122	3.28
	1-*E,Z*	353	32883	3.26
	1-*Z,Z*	366	58167	3.18
Dichloromethane	1-*E,E*	339	56056	3.30
	1-*E,Z*	349	42500	3.27
	1-*Z,Z*	363	33722	3.21
Acetone	1-*E,E*	339	40389	3.33
	1-*E,Z*	349	39944	3.30
	1-*Z,Z*	357	49000	3.25

The molar absorptivity for all the bands presented in the UV spectra of the isomers (see SI) confirms the assigned π-π* transitions, since all are up to 10^4 cm^{-1} M^{-1}.[61] The HOMO-LUMO band gaps also confirm, as expected, the decrease on the energy levels involved in the transitions, however one notes the thermodynamic stabilization brought by the intermolecular hydrogen bond. We also observed that the energy band gaps, for each isomer in the three different solvents, increase as the polarity of the solvents increases, which can also be seen in small hypsochromic shifts for each of the three isomers between 1-9 nm for all the bands in the spectra. For spectra taken in acetone, we were able just to compare the λ_{max} due to the large cut off of this solvent. Even though the formation of an intramolecular hydrogen bond may extend the conjugation of the system, the tendency to form hydrogen bonds between solvent molecules and non-bonding electrons of the isomers,[61,62] may stabilize the low-lying *n* orbitals, resulting in a higher transition energy.

Redox Behaviour: Cyclic Voltammetry (CV) and Oster Young Squared Wave Voltammetry (OSWV) were conducted in DMF with NBu_4PF_6 as supporting electrolyte, using a 3-mm-diameter glassy carbon disk as the working electrode, a silver wire as a pseudoreference electrode and a platinum wire as a counter electrode. Ferrocene was added at the end of the experiments, and used as internal reference for measuring the potentials.

The CV and OSWV of compound **1** and its isomers show two irreversible oxidation potentials. Presumably, these oxidation steps are attributable to the N-H oxidation of both arms.[63] As we go from the *E,E* to the *Z,Z* configurations it is observed an anodic shift (see Figure 12) which suggest a small decrease in the acidity of the N-H protons due to the formation of the intramolecular hydrogen bond with the lateral pyridine ring. This fact is confirmed by X-ray studies and DFT calculations (see above) as well.

On the other hand, the three isomers exhibit irreversible reduction potentials (see Figure 12). Higher scan rates do not appreciably change the difference of the peak potentials in the cyclic voltammogram. Table 4 compiles the peak potentials of the three isomers. Additionally, a linear relationship between I_c and $v^{1/2}$ is observed, which indicates that reductions are controlled by diffusion.

Interestingly, the reduction occurring on the imine group is cathodically shifted as the intramolecular hydrogen bond is formed (see Figures 12 and 13). In fact it goes from -1.86 V to -2.25 V, a 390 mV shift due to the larger hindrance of the –N-H group in the **1-*Z,Z*** isomer.

Table 4. Peak potentials for the cathodic and anodic events of isomers **1-*E,E***, **1-*E,Z*** and **1-*Z,Z***.

Isomer	$E_{p, oxd(1)}$	$E_{p, oxd(2)}$	$E_{p, red(1)}$	$E_{p, red(2)}$	$E_{p, red(3)}$	$E_{p, red(4)}$	$E_{p, red(5)}$	$E_{p, red(6)}$
1-*E,E*	0.77	0.95	-1.86	-2.39	-2.57	-2.83	-3.06	-3.33
1-*E,Z*	0.79	0.96	-1.83	-2.20	-2.35	-2.48	-2.99	-3.22
1-*Z,Z*	0.89	1.07		-2.25	-2.32	-2.50	-2.94	-3.23

10.1002/chem.201703065

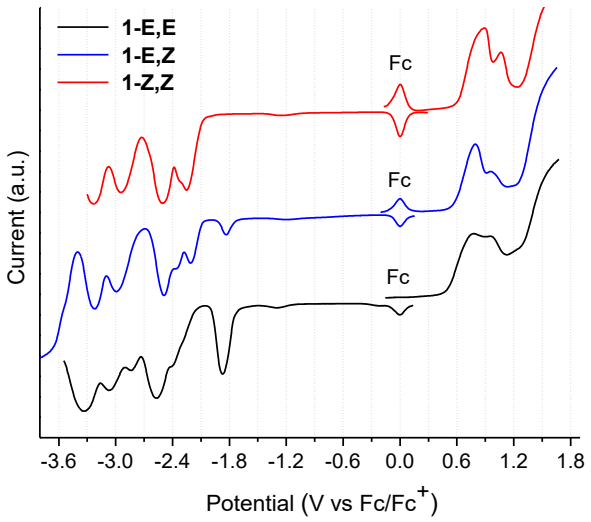

Figure 12. OSWV of **1-*E,E*** and its ***E,Z*** and ***Z,Z*** isomers in NBu_4PF_6/DMF with ferrocene as the internal standard, 100 mV/s scan rate.

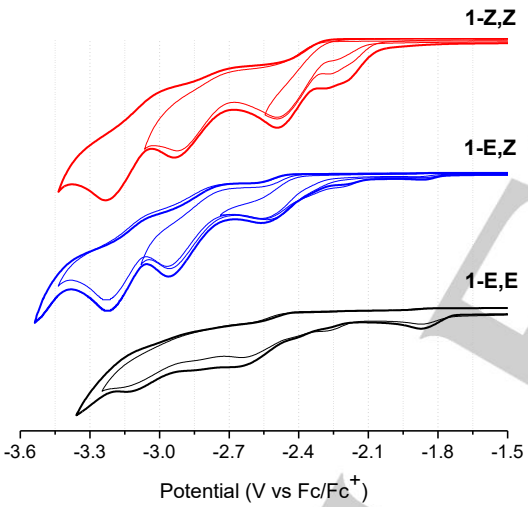

Figure 13. CV of **1** and its *E,Z* and *Z,Z* isomers in NBu_4PF_6/DMF with ferrocene as the internal standard, 100 mV/s scan rate.

On the other hand, we found that electrolysis (under inert atmosphere) of the **1-*Z,Z*** isomer at -2,25 V followed by reoxidation yields exclusively the **1-*E,E*** isomer which is accompanied by a color change, going from translucent to light yellow (see SI, Figure S12). The same results are also obtained by running several cyclic voltammograms in anodic potentials (Figure 14), suggesting that the amine hydrogen plays an important role during the mechanism of reduction of the imine. Presumably, the carbon anion radical (upon reduction) delocalizes the transferred electron throughout the N-N(H) moiety, thus, the larger acidity of the **1-*E,E*** isomer facilitates this process and therefore, an easier reduction is observed compared to its **1-*E,Z*** and **1-*Z,Z*** counterparts.

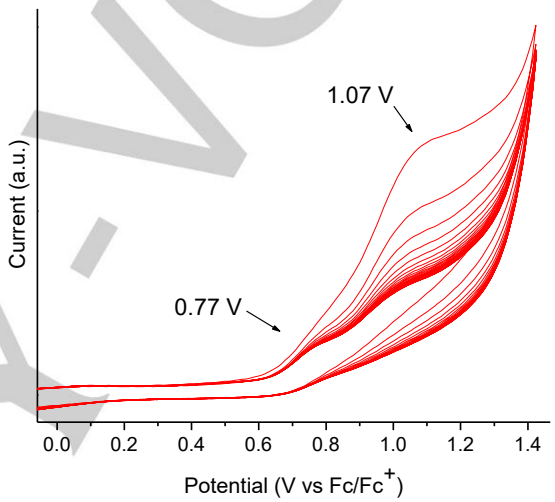

Figure 14. CV of **1-*Z,Z*** after several voltammetric cycles. 100 mV/s scan rate.

Final remarks -Photo-electrochemical switch: We have shown that compound **1-*E,E*** may undergo photo-induced isomerization to **1-*E,Z*** or **1-*Z,Z***. Additionally, each of these states are stable enough to be isolated and characterized by NMR, UV-Vis, electrochemistry and X-ray crystal diffraction. DFT calculations and NMR confirm the importance of the amine proton, which is involved in an intramolecular hydrogen bond with the nitrogen from the pyridine ring. This hydrogen bond (in both *E,Z* and *Z,Z* isomers) can be broken by applying an electrochemical potential, and therefore, the **1-*E,E*** state can be reestablished (Scheme 2).

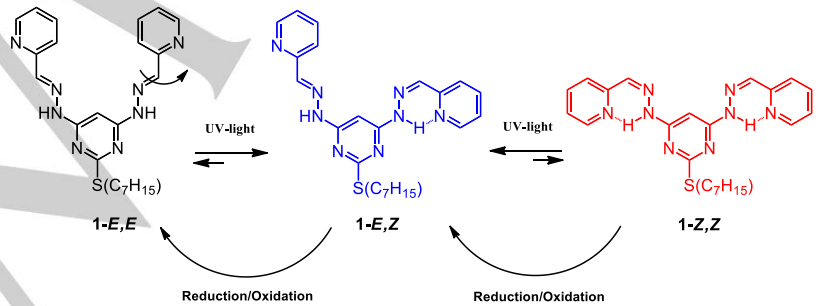

Scheme 2. Representation of the electrochemical switching from the isomers **1-*Z,Z*** and **1- *E,Z*** to the isomer **1-*E,E***.

In this regard, bis(hydrazone) **1-*E,E*** works as a photo-electrochemical switch, being activated by UV-light and reestablished by electrochemical potentials. For the best of our knowledge, this is the first double hydrazone switch responding to two different external stimuli.

Conclusions

A symmetrical two-arm system based on a pyridine-hydrazone-thiopyrimidine framework underwent configurational dynamics by photo-induced *E*-to-*Z* isomerization in both arms following reversible consecutive steps. The rates of isomerization calculated and the kinetic studies showed that upon UV irradiation the equilibria are shifted towards the **1-*E,Z*** isomer.

The configurational dynamics of the isomer **1-*E,E*** allowed to isolate and characterize by experimental techniques and theoretical calculations the configurational isomers **1-*E,Z*** and **1-*Z,Z***, which proved to be highly stable by the intramolecular hydrogen bond formed. The photochemical, electrochemical and structural studies of the double hydrazone carried out in this work allowed to identify metastable states and potential use in photochemical applications, such as photo-electrochemical switches, photo/electrochemically activated-carriers, and in photochemical assisted synthesis of supramolecular entities.

Experimental Section

General: Starting materials were purchased from Sigma-Aldrich and were used without further purification. For Thin Layer Chromatography (TLC) it was used 60 F_{254} (0.25 mm) silica gel to verify the purity of the products and to monitor the separation by column chromatography. In order to reveal the TLC, it was used a lamp Spectroline Serie E with a wavelength of 363 nm. Column Chromatography (CC) was performed for the purification of the products using 230-400 mesh silica gel particles.

Solution ^{1}H (400 MHz) and ^{13}C (100 MHz) NMR spectra were recorded with a Bruker UltraShield spectrometer at 25 °C, using deuterated solvents as $CDCl_3$ and Acetone–d_6. Chemical shifts are quoted in ppm relative to tetramethylsilane, using the residual solvent peak as a reference. The following notation is used for the ^{1}H NMR spectral splitting patterns: singlet (s), doublet (d), triplet (t), quintuplet (q), multiplet (m). 2D–NMR used experiments were Heteronuclear single–quantum correlation spectroscopy (HSQC), Heteronuclear multiple–bond correlation spectroscopy (HMBC) and Correlation Spectroscopy (COSY).

UV–Vis spectra were recorded on UV–1700 PharmaSpec Shimadzu spectrophotometer and melting point measures were performed in a Stuart SMP3 melting point apparatus. Electrochemical studies were performed in a CHI760B CH instruments potentiostat, respectively. All spectroscopy samples were taken at room temperature.

Photoisomerization of 1-*E,E* and 1-*Z,Z*: Solutions of the isomers in NMR Quartz tubes were placed at 20 cm away from a mercury vapour lamp and were irradiated. The photoisomerization processes were monitored through time by NMR spectroscopy.

Actinometry: We determined light intensity of a 250-Watts Mercury Vapour Lamp using a micro version of the "Hatchard and Parker's method" suggested by Fisher of the potassium ferrioxalate actinometer (see SI).[64]

Isolation of the isomers 1-*E,Z* and 1-*Z,Z*: A 26.75 mmol.L^{-1} solution of the bis(hydrazone) **1-*E,E*** in a NMR Quartz tube was placed at 20 cm away from a 250W mercury-vapour lamp, and irradiated during 70 min in order to obtain the isomers. Each isomer obtained from the UV irradiation of the bishydrazone **1-*E,E*** in commercial acetone was isolated by column chromatography using a gradient of elution from $CHCl_3$ to $CHCl_3$/MeOH 3%. The NMR spectra of the three isomers were taken in $CDCl_3$ and acetone-d_6. The assignments are supported by 2D NMR experiments (COSY and HSQC; see SI).

(*E,Z*)–Pyridine–2–carboxaldehyde–[2–heptylthiopyrimidine–4,6–diyl]bishydrazone (1-*E,Z*): Bishydrazone **1-*E,Z*** was isolated with 67% yield. M.p.: 178.4-180.9 °C; ^{1}H NMR (400 MHz, $CDCl_3$), δ/ppm: 13.98 (s, 1H), 8.71 (d, *J* = 4.4 Hz, 1H), 8.58 (s, 2H), 8.10 (d, *J* = 8.0 Hz, 1H), 7.90 (s, 1H), 7.84-7.80 (m, 1H), 7.75-7.71 (m, 1H), 7.40 (d, *J* = 7.9 Hz, 1H), 7.31-7.28 (m, 2H), 7.26-7.22 (m, 1H), 6.94 (s, 1H), 3.13 (t, *J* = 7.3 Hz, 2H), 1.78-1.71 (m, 2H), 1.50-1.43 (m, 2H), 1.37 – 1.25 (m, 6H), 0.88 (t, *J* = 6.6 Hz, 3H). ^{13}C NMR (100.60 MHz, $CDCl_3$) δ/ppm: 170.6, 162.7, 161.5, 153.1, 149.4, 148.3, 141.9, 137.2, 136.5, 133.0, 124.9, 123.6, 123.2, 120.5, 79.9, 77.3, 31.9, 30.9, 29.7, 29.1, 29.0, 22.8, 14.2. Elemental analysis calcd (%) for $C_{27}H_{40}N_8O_2S$ (**1-*E,Z*** 2EtOH): C 59.97, H 7.46, N 20.72, O 5.92; found: C 59.93, H 7.42, N 20.70, O 5.92.

(*Z,Z*)–Pyridine–2–carboxaldehyde–[2–heptylthiopyrimidine–4,6–diyl]bishydrazone (1-*Z,Z*): Bishydrazone **1-*Z,Z*** was isolated with 20% yield. M.p.: 166.5-167.8 °C; ^{1}H NMR (400 MHz, Acetone-d_6), δ/ppm: 14.01 (s, 2H), 8.80 (d, *J* = 3.9 Hz, 2H), 8.05 (t, *J* = 7.5 Hz, 2H), 7.72 (d, *J* = 7.8 Hz, 2H), 7.53-7.50 (m, 2H), 7.45 (s, 2H), 7.02 (s, 1H), 3.15 (t, *J* = 7.3 Hz, 2H), 1.80-1.77 (m, 2H), 1.55-1.51 (m, 2H), 1.42-1.35 (m, 6H), 0.88 (s, 3H). ^{13}C NMR (100.60 MHz, $CDCl_3$) δ /ppm: 153.2, 148.3, 137.2, 136.5, 124.8, 123.1, 79.7, 77.3, 31.9, 30.9, 29.8, 29.1, 29.0, 22.8, 14.2.

X-Ray Crystallographic studies: All single-crystal X-ray data at room temperature (296 K) were collected on a Bruker APEX-II CCD diffractometer using MoKα radiation (0.71073 Å) monochromated by graphite. The cell determination and the final cell parameters were obtained on all reflections using the software Bruker SAINT[65] included in APEX2 software suite[66]. Data integration and scaled was carried out using the software Bruker SAINT.[65] Considering the disorder problems in the refinement of the **1-*E,Z*** isomer, single-crystal X-ray data were also collected at low temperature (110 K) on an Enraf-Nonius Kappa-CCD diffractometer using MoKα radiation (0.71073 Å) monochromated by graphite. The cell determination and the final cell parameters were obtained on all reflections using the software Collect and Scalepack[67]. Data integration and scaled was executed using the software Denzo-SMN and Scalepack.[68]

The structures were solved using the software SHELXS-2013 and refined using SHELXL-2013,[69] contained in WinGX[70] and Olex2-1.2.[71] Non-hydrogen atoms of the molecules were clearly resolved and full-matrix least-squares refinements of these atoms with anisotropic thermal parameters were performed. Positional disordered atoms were refined in two different positions per disordered atom using PART instruction. All hydrogen atoms including those belonging to disordered atoms were stereochemically located and refined with the riding model.[69] Hydrogen atoms bonded to N atoms were identified in the density map. ORTEP diagram was generated with OLEX2[71]. Mercury software[72] was used to prepare the illustrations. The structural analysis of **1-*E,Z*** isomer was performed with data collected at 100 K. Crystal data collection and structure refinement details are summarized in Table S1 (see SI).

Electrochemistry of the bishydrazone isomers: Electrochemical experiments were carried out in a 0.1 mol.L^{-1} solution of Bu_4PF_6 in DMF in a classical three-electrode cell, connected to a computerized electrochemical device AUTOLAB M101. The working electrode was a glassy carbon disc (3 mm diameter), the auxiliary electrode a platinum wire, the reference electrode silver wire, and as internal standard was used ferrocene. The measurements were carried out by cyclic and square wave voltammetry.

Theoretical calculations: Theoretical calculations were carried out using Gaussian 09[73] and GaussView 5[74] as graphic interphase running on Windows, using Density Functional Theory methods and B3LYP: 6-311+G (d, p) basis set for Geometry optimization and single-point energy calculations. Vibrational frequencies calculations were computed at same level of theory in order to ascertain that the global minima were achieved in each structure optimization.

Acknowledgements

Authors are grateful to the Vicerrectoría de Investigaciones and the Centro de Excelencia en Nuevos Materiales (CENM) from the Universidad del Valle (Colombia) as well as El Departamento Administrativo de Ciencia, Tecnología e Innovación (COLCIENCIAS) for the financial support of this work. M.S-M. and R. D. acknowledge to Coordenação de Aperfeiçoamento de Pessoal de Nível Superior and Conselho Nacional de Desenvolvimento Científico y Tecnológico for the CNPq and CAPES/PNPD scholarship from Brazilian Ministry of Education and R. de Almeida Santos to facilitate the measurements and FAPESP (2009/54011-8) for providing Apex-II equipment. M.C. thanks the University of Strasbourg for a post-doctoral fellowship.

Keywords: Bis(hydrazone), configurational isomers, photoisomerization, supramolecular chemistry, thiopyrimidine

[1] A. Samoson, T. Tuherm, J. Past, A. Reinhold, T. Anupõld, I. Heinmaa, A. Meijere, K. N. Houk, H. Kessler, J. M. Lehn, et al., *Molecular Machines*, Springer Berlin Heidelberg, **2005**.

[2] V. Balzani, A. Credi, F. M. Raymo, J. F. Stoddart, *Angew. Chem. Int. Ed.* **2000**, *39*, 3348–3391.

[3] S. Erbas-Cakmak, D. A. Leigh, C. T. McTernan, A. L. Nussbaumer, *Chem. Rev.* **2015**, *115*, 10081–10206.

[4] V. Balzani, A. Credi, M. Venturi, in *Mol. Devices Mach. Concepts Perspect. Nanoworld*, WILEY-VCH, Weinheim, Germany, **2008**, pp. 1–21.

[5] S. C. Burdette, *Nat. Chem.* **2012**, *4*, 695–696.

[6] E. Romero, F. Zuluaga, R. D`vries, M. N. Chaur, *J. Brazilian Chem. Soc.* **2015**, *0*, 1–9.

[7] B. L. Feringa, *J. Org. Chem.* **2007**, *72*, 6635–6652.

[8] T. R. Kelly, M. C. Bowyer, K. V. Bhaskar, D. Bebbington, A. Garcia, F. Lang, M. H. Kim, M. P. Jette, *J. Am. Chem. Soc.* **1994**, *116*, 3657–3658.

[9] W. R. Browne, B. L. Feringa, *Nat. Nanotechnol.* **2006**, *1*, 25–35.

[10] M. A. Watson, S. L. Cockroft, *Chem. Soc. Rev.* **2016**, DOI 10.1039/C5CS00874C.

[11] J. E. Green, J. W. Choi, A. Boukai, Y. Bunimovich, E. Johnston-Halperin, E. DeIonno, Y. Luo, B. a Sheriff, K. Xu, Y. S. Shin, et al., *Nature* **2007**, *445*, 414–7.

[12] P. Ceroni, A. Credi, M. Venturi, V. Balzani, *Photochem. Photobiol. Sci.* **2010**, *9*, 1561–1573.

[13] E. R. Kay, D. A. Leigh, F. Zerbetto, *Angew. Chemie - Int. Ed.* **2007**, *46*, 72–191.

[14] W. S. Tan, P. Y. Chuang, C. H. Chen, C. Prabhakar, S. J. Huang, S. L. Huang, Y. H. Liu, Y. C. Lin, S. M. Peng, J. S. Yang, *Chem. - An Asian J.* **2015**, *10*, 989–997.

[15] J.-M. Lehn, *Chem. Eur. J.* **2006**, *12*, 5910–5915.

[16] X. Su, I. Aprahamian, *Chem. Soc. Rev.* **2014**, *43*, 1963–81.

[17] X. Y. Cao, J. Harrowfield, J. Nitschke, J. Ramírez, A. M. Stadler, N. Kyritsakas-Gruber, A. Madalan, K. Rissanen, L. Russo, G. Vaughan, et al., *Eur. J. Inorg. Chem.* **2007**, 2944–2965.

[18] L. N. Dawe, T. S. M. Abedin, L. K. Thompson, *Dalton Trans.* **2008**, *2*, 1661–1675.

[19] N. Parizel, J. Ramírez, C. Burg, S. Choua, M. Bernard, S. Gambarelli, V. Maurel, L. Brelot, J.-M. Lehn, P. Turek, et al., *Chem. Commun.* **2011**, *47*, 10951.

[20] J. G. Hardy, *Chem. Soc. Rev.* **2013**, *42*, 7881–99.

[21] D. J. Hutchinson, L. R. Hanton, S. C. Moratti, *Inorg. Chem.* **2010**, *49*, 5923–5934.

[22] D. J. Hutchinson, L. R. Hanton, S. C. Moratti, *Inorg. Chem.* **2011**, *50*, 7637–7649.

[23] M. N. Chaur, D. Collado, J.-M. Lehn, *Chem. An Eur. J.* **2011**, *17*, 248–58.

[24] M. A. Gordillo, M. Soto-Monsalve, G. Gutiérrez, R. F. D'vries, M. N. Chaur, *J. Mol. Struct.* **2016**, *1119*, 286–295.

[25] M. Ruben, J. Lehn, G. Vaughan, *Chem. Commun.* **2003**, *3*, 1338–1339.

[26] M. A. Fernandez, J. C. Barona, D. Polo-Cerón, M. N. Chaur, *Rev. Colomb. Química* **2014**, *43*, 5–11.

[27] J. Holub, G. Vantomme, J. M. Lehn, *J. Am. Chem. Soc.* **2016**, *138*, 11783–11791.

[28] G. Gutiérrez, M. Gordillo, M. N. Chaur, *Rev. Colomb. Química* **2016**, *45*, 28–32.

[29] G. Vantomme, S. Jiang, J. M. Lehn, *J. Am. Chem. Soc.* **2014**, *136*, 9509–9518.

[30] X. Su, T. Lessing, I. Aprahamian, *Beilstein J. Org. Chem.* **2012**, *8*, 872–876.

[31] I. Aprahamian, *Nat. Chem.* **2015**, *8*, 97–99.

[32] J. Leblond, A. Petitjean, *ChemPhysChem* **2011**, *12*, 1043–1051.

[33] M. J. Barrell, A. G. Campaña, M. Von Delius, E. M. Geertsema, D. A. Leigh, *Angew. Chemie - Int. Ed.* **2011**, *50*, 285–290.

[34] G. Gil-Ramírez, D. a. Leigh, A. J. Stephens, *Angew. Chemie Int. Ed.* **2015**, *54*, 6110–6150.

[35] A.-M. Stadler, N. Kyritsakas, R. Graff, J.-M. Lehn, *Chem. An Eur. J.* **2006**, *12*, 4503–22.

[36] M. Ruben, J. Rojo, F. J. Romero-Salguero, L. H. Uppadine, J.-M. Lehn, *Angew. Chemie Int. Ed.* **2004**, *43*, 3644–3662.

[37] M. A. Gordillo, F. Zuluaga, M. N. Chaur, *Rev. Colomb. Química* **2016**, *45*, 39–50.

[38] L. Greb, J.-M. Lehn, *J. Am. Chem. Soc.* **2014**, *136*, 13114–13117.

[39] L. Greb, A. Eichhöfer, J.-M. Lehn, *Angew. Chemie Int. Ed.* **2015**, *54*, 14345–14348.

[40] S. M. Landge, E. Tkatchouk, D. Benítez, D. A. Lanfranchi, M. Elhabiri, W. a Goddard, I. Aprahamian, *J. Am. Chem. Soc.* **2011**, *133*, 9812–23.

[41] M. N. Chaur, *Rev. Colomb. Química* **2012**, *41*, 349–358.

[42] C. C. Carmona-Vargas, I. Y. Váquiro, L. M. Jaramillo-Gómez, J.-M. Lehn, M. N. Chaur, *Inorganica Chim. Acta* **2017**, DOI 10.1016/j.ica.2017.05.002.

[43] P. Kuzmic, *Anal. Biochem.* **1996**, *237*, 260–273.

[44] M. A. Spackman, J. J. McKinnon, *CrystEngComm* **2002**, *4*, 378–392.

[45] J. J. McKinnon, M. A. Spackman, A. S. Mitchell, *Acta Crystallogr. B.* **2004**, *60*, 627–668.

[46] J. J. McKinnon, D. Jayatilaka, M. A. Spackman, *Chem. Commun.* **2007**, 3814–3816.

[47] M. M. Deshmukh, S. R. Gadre, L. J. Bartolotti, *J. Phys. Chem. A* **2006**, *110*, 12519–12523.

[48] D. Stöckl, K. Dewitte, L. M. Thienpont, *Clin. Chem.* **1998**, *44*, 2340–2346.

[49] D. R. Flower, *J. Mol. Graph. Model.* **1999**, *17*, 238–244.

[50] P. Gilli, L. Pretto, V. Bertolasi, G. Gilli, *Acc. Chem. Res.* **2009**, *42*, 33–44.

[51] K. H. Møller, A. S. Hansen, H. G. Kjaergaard, *J. Phys. Chem. A* **2015**, *119*, 10988–10998.

[52] M. R. Preimesberger, A. Majumdar, S. L. Rice, L. Que, J. T. J. Lecomte, *Biochemistry* **2015**, *54*, 6896–6908.

[53] S. G. Estácio, P. Cabral do Couto, B. J. Costa Cabral, M. E. Minas da Piedade, J. A. Martinho Simões, *J. Phys. Chem. A* **2004**, *108*, 10834–10843.

[54] M. M. Deshmukh, C. H. Suresh, S. R. Gadre, *J. Phys. Chem. A* **2007**, *111*, 6472–6480.

[55] M. Jabłoński, A. Kaczmarek, A. J. Sadlej, *J. Phys. Chem. A* **2006**, *110*, 10890–10898.

[56] D. Rusinska-Roszak, *J. Phys. Chem. A* **2015**, *119*, 3674–3687.

[57] A. Laventure, G. De Grandpre, A. Soldera, O. Lebel, C. Pellerin, *Phys. Chem. Chem. Phys.* **2016**, *18*, 1681–1692.

[58] J.-L. Schmitt, A.-M. Stadler, N. Kyritsakas, J.-M. Lehn, *Helv. Chim. Acta* **2003**, *86*, 1598–1624.

[59] B. Vickery, G. R. Willey, M. G. B. Drew, *J. Chem. Soc. Perkin Trans. 2* **1981**, 155.

[60] F. Kaberia, B. Vickery, G. R. Willey, M. G. B. Drew, *J. Chem. Soc. Perkin Trans. 2* **1980**, 1622.

[61] L. D. S. Yadav, *Organic Spectroscopy*, Springer Science & Business Media, **2013**.

[62] J. Mohan, *Organic Spectroscopy: Principles and Applications*, CRC Press, **2004**.

[63] A. Adenier, M. M. Chehimi, I. Gallardo, J. Pinson, N. Vilà, *Langmuir* **2004**, *20*, 8243–8253.

[64] M. Montalti, A. Credi, L. Prodi, M. T. Gandolfi, *Handbook of Photochemistry.*, CRC Press, Boca Ratón, Florida, **2006**.

[65] *SAINT*, Bruker AXS Inc., Madison, Wisconsin,USA, **2012**.

[66] *APEX2*, Bruker AXS Inc., Madison, Wisconsin,USA, **2012**.

[67] *COLLECT*, Nonius BV, Delft, The Netherlands, **1998**.

[68] Z. Otwinowski, W. Minor, in (Ed.: B.-M. in Enzymology), Academic Press, **1997**, pp. 307–326.

[69] G. M. Sheldrick, *Acta Crystallogr. Sect. C Struct. Chem.* **2015**, *71*, 3–8.

[70] L. J. Farrugia, *J. Appl. Crystallogr.* **2012**, *45*, 849–854.

[71] O. V Dolomanov, L. J. Bourhis, R. J. Gildea, J. A. K. Howard, H. Puschmann, *J. Appl. Crystallogr.* **2009**, *42*, 339–341.

[72] C. F. Macrae, I. J. Bruno, J. A. Chisholm, P. R. Edgington, P. McCabe, E. Pidcock, L. Rodriguez-Monge, R. Taylor, J. van de Streek, P. A. Wood, *J. Appl. Crystallogr.* **2008**, *41*, 466–470.

[73] M. J. Frisch, G. W. Trucks, H. B. Schlegel, G. E. Scuseria, M. A. Robb, J. R. Cheeseman, G. Scalmani, V. Barone, B. Mennucci, G. A. Petersson, et al., **2009**.

[74] R. Dennington, T. Keith, J. Millam, **2009**.

10.1002/chem.201703065

WILEY-VCH

FULL PAPER